UNCONVENTIONAL RESOURCES TECHNOLOGY CONFERENCE
FUELED BY SPE • AAPG • SEG

URTeC: 3723620

Optimizing Well Spacing and Completion Design Using Simulation Models Calibrated to the Hydraulic Fracture Test Site 2 (HFTS-2) Dataset

Sriram Pudugramam[1], Rohan J. Irvin[*2], Mark McClure[2], Garrett Fowler[2], Fadila Bessa[1], Yu Zhao[1], Jichao Han[1], Han Li[1], Arjun Kohli[3], Mark D. Zoback[3], 1. Occidental, 2. ResFrac Corporation, 3. Stanford University.

Abstract

This paper presents a calibration and optimization workflow using a fully coupled hydraulic fracturing, reservoir, and geomechanics simulator, as applied to the HFTS-2 dataset in the Delaware Basin, Texas, USA. Modeling began with building a geomechanical stress profile using the viscoelastic stress relaxation (VSR) method. The model was then calibrated to key observations from the field diagnostic data, which included: horizontal and vertical well DAS/DTS/DSS fiber, downhole microseismic arrays, pressure gauges, core-through data, image logs, DFITs, proppant-in-cuttings analysis, interference tests, and production data. Finally, the calibrated model was used to perform an economic optimization of design parameters by running hundreds of variations and comparing their performance. Model calibration required adjustment of global parameters for fracture toughness, leakoff, and viscous pressure drop, as well as fracture toughness in a few specific layers. Production and depletion observations were matched by adjusting a global permeability multiplier, relative permeability curves, and pressure-dependent permeability reduction with depletion. Only the toe sections of the child well(s) were overlapping with the depleted zone from parent wells. This allowed the model to be calibrated to data from both the un-depleted and depleted parts of the well, where the latter was observed to have more lateral asymmetry.

The ‘best case’ simulation from the optimization algorithm has a 60% increase in NPV/section over the base case design. Sensitivity analysis on economic performance found that spacing and landing zone are the primary drivers of performance due to their impact on effective drainage area. Proppant loading and cluster spacing were also performance drivers due to their contribution to fracture conductivity and effective fracture length.

The comprehensive dataset that was used for model calibration enables an extremely well-constrained model, improving confidence in the model’s predictions. The applied workflow demonstrates how physical insights and understanding of fundamental performance mechanisms allow for the prescriptive design of horizontal fractured wells in shale basins.

Introduction

Economic optimization of is a primary objective for operators developing tight hydrocarbon resources. As the industry matures and developments move into new areas, the ability to continuously determine the optimal development scheme (well spacing, landing depth and completion design) is of critical importance. This work leverages the detailed dataset from the Hydraulic Fracture Test Site-2 (HFTS-2) to build a calibrated model. The model can simulate hundreds of different development schemes to evaluate the optimal development strategy. Model-driven predictions can be field tested in future developments. Guidance from modeling increases the likelihood of success for the field trials, accelerating the learning curve and increasing the value operators can extract from their acreage positions.

HFTS-2 is a cost-shared, field-scale R&D program in the Permian (Delaware) Basin. Figure 1 shows the location of the HFTS-2 project in the Delaware Basin, which is about 140 miles west of the HFTS-1 project area. Occidental is the host and operator of the HFTS-2 project with Shell being a joint venture partner. The US Department of Energy (DOE) through the National Energy Technology Laboratory (NETL) and 16 consortia members have funded about $30 million for science data acquisition and interpretation to perform hydraulic fracturing research.

In the HFTS-2, two parent horizontal Bitterroot wells (BR1H and BR2H) were drilled and completed three years before the child wells, four horizontal Boxwood wells (BX1H, BX2H, BX3H, and BX4H) with over 100 stimulated stages and varying completion designs spanning the Wolfcamp-X to Wolfcamp-A formations. The average lateral length of the parent wells is 60% of the four child wells, which offers a clear distinction between the stages influenced by parent-child effects and the stages without any depletion effects. The asymmetry in fracture geometry, which influences well spacing and landing decisions, is a critical piece of the puzzle to optimize capital expenditure and reduce the environmental footprint of the unconventional resources industry.

The HFTS-2 project also includes a vertical pilot well (BX5PH) drilled before the child well stimulation, and a slant core well (BX6S) drilled after the child well stimulation. In general, the project area can be separated into a North sector and a South sector (see Figure 2). The South sector includes the parent wells where depletion or parent-child effects come into play. The North sector contains the two data collection wells (BX5PH and BX6S) and has no offset parent wells.

The HFTS-2 project provides a unique opportunity to improve our understanding of the hydraulic fracturing process in unconventional reservoirs. The primary objectives include: a) evaluate various completion designs; b) characterize HF geometry/dimensions and resulting depletion profiles, with and without parent wells' influence; c) identify and test new technologies; and d) build a comprehensive hydraulic fracturing diagnostics dataset. Additional background information on the HFTS-2 project is described by Ciezobka (2021).

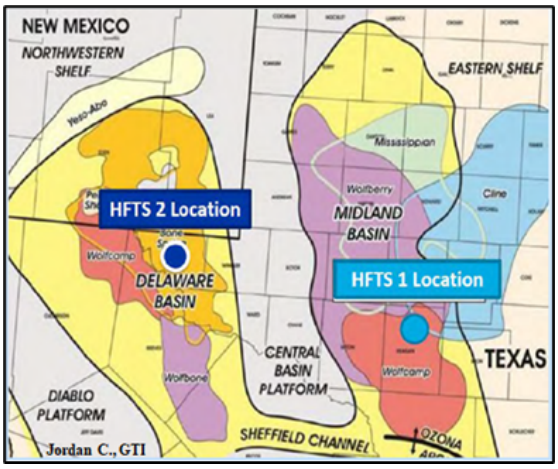

Figure 1. Location of the HFTS-2 project

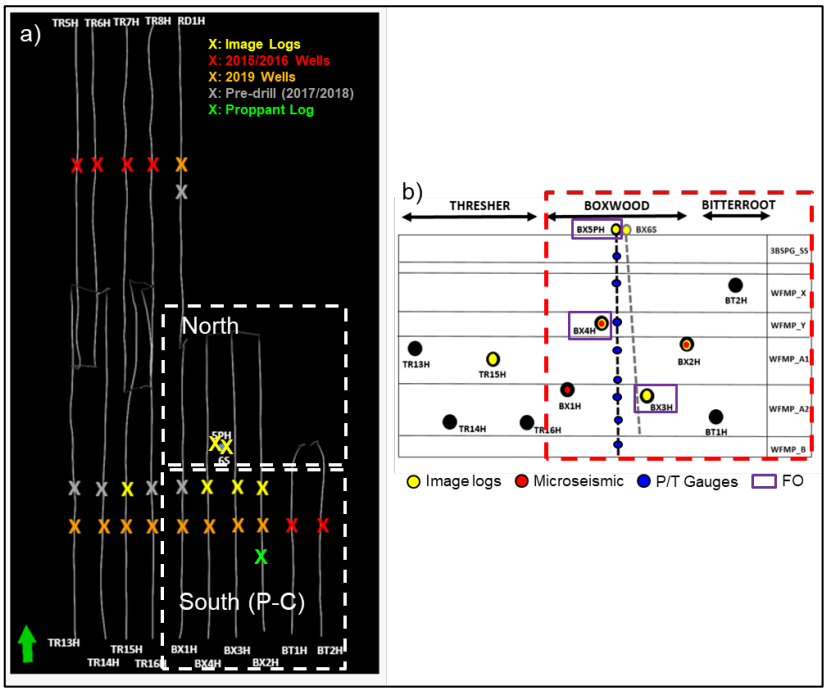

Figure 2 Schematic of the HFTS-2 wells: a) Plan view, b) Gun barrel view

HFTS-2 Dataset Overview

The comprehensive diagnostic datasets acquired in the HFTS-2 project include microseismic (MS), ~540 ft of core from the vertical pilot hole (BX5PH), ~950 ft of SRV core from the slant well (BX6S), diagnostic formation injection tests (DFIT), PVT, quad combo and image logs, proppant logs, timelapse geochemistry, 28 P/T gauges data in the production and science wells, varying completion designs, and permanent fiber optic (FO) cable in two horizontal wells (BX3H and BX4H) and one vertical well (BX5PH). Figure 3 provides an overview of the HFTS-2 dataset. The integration and analysis of the HFTS-2 comprehensive dataset and project key learnings can be found in Pudugramam et al. (2021) and Zhao et al. (2021).

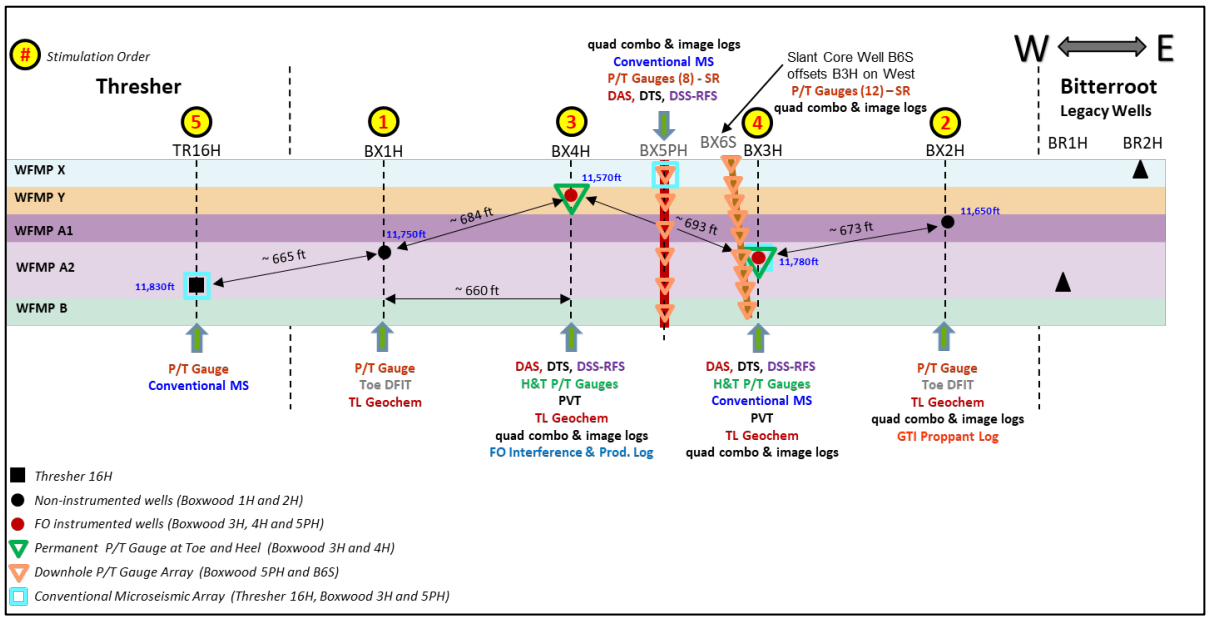

Figure 3 Overview of the HFTS-2 dataset

Microseismic Data

In the HFTS-2, five separate multi-geophone arrays were deployed on BX3H, BX5PH and TR16H to acquire a very comprehensive microseismic dataset during the stimulation of BX1H, BX2H and BX4H. The infill wells, which were treated sequentially, exhibited very different patterns of microseismicity depending on whether they were offset prior depletion.

There was preferential eastward growth of events during the stimulation of BX1H and BX2H toe stages that overlap the two parent wells BR1H and BR2H. This is likely due to the influence of the depleted area around the parent wells. Most of the seismicity is vertically constrained from top of Wolfcamp formation to Wolfcamp-B though microseismic events are consistently observed as high as the 2nd Bone Springs. A full description of the microseismic acquisition and processing is provided by Grechka et al. (2021).

Pre- and Post-Stimulation Logs and Core Data

Before drilling and completion of the horizontal Boxwood wells, about 540 ft of whole core and advanced logs were acquired from the vertical pilot well BX5PH. Special core measurement techniques were used to distinguish rock types, and the openhole well logs provided critical subsurface properties.

About 950 ft of SRV core was acquired from the slant well BX6S in nine coring runs with a close approach to the BX3H wellbore. Through comprehensive core analysis and fracture description, a total of 1261 fractures, including 500 hydraulic fractures, were described in 948 feet of core. The hydraulic fractures were shown to be planar with the SHmax orientation of 80°, which was confirmed by microseismic data, fiber optic data, and a regional sonic azimuthal anisotropy study. A detailed description of the slant core is provided by Gale et al. (2021).

Image logs were also acquired on BX2H, BX3H, BX4H, BX5PH, and BX6S. Specifically, the image log on BX2H, which was obtained before stimulation of the child wells but after the parent wells' stimulation, show two distinct fracture sets (i.e., NE-SW oriented resistive fractures, and hydraulic-induced conductive fractures oriented around 80°). The intensity of conductive fractures along the lateral of BX2H was contrasted between North and the South sectors. The intensity of conductive fractures is greater in the Southern sector, indicating impacts from the parent wells' stimulation. This observation was corroborated by the GTI proprietary proppant log, which analyzed the spatial distribution of proppant

sand particles in the drilling mud returns for child wells (Maity and Ciezobka, 2021). The log and core interpretation as related to the integration with other datasets are provided by Bessa et al. (2021).

Completion Designs and DFIT Data

The primary objective of the Design of Experiments (DoE) for the HFTS-2 project was to evaluate the stimulation distribution effectiveness (SDE) of various stimulation schemes relative to a baseline configuration. This baseline had a ~190 ft geometric stage length (SL) containing 6 perforation clusters (PC) with a perforation cluster spacing (PCS) of 32 ft. Each PC had 4 perforations for a total of 24 perforations per stage, and each perforation had an average entry hole diameter (EHD) of 0.41 in. This baseline configuration is compared to more Aggressive Limited Entry (ALE) practices achieved by reducing the number of perforations per cluster. Additionally, tapered perforations to reduce heel-side bias were tested along with Extended Stage Length (ESL) with 10 PCs per stage at ~330 ft SL using ALE practices. In the HFTS-2, the horizontal Boxwood wells were stimulated through single-well operations, or "stack fracs." BX1H was stimulated first, followed by BX2H second and BX4H third. Then the MS array in BX3H was retrieved prior to its stimulation. More detailed description of the HFTS-2 completion designs can be found in Zakhour et al., 2021.

DFITs were performed in BX1H, BX2H, TR13H, TR14H and TR15H. The acquired DFIT data was analyzed to estimate Shmin, pore pressure and matrix permeability, which are critical parameters for fracture modelling and reservoir simulation. The BX2H DFIT interpretation yielded a significantly lower pore pressure estimate than all the other DFITs. This is likely because the fracture created by the BX2H DFIT being near a depleted hydraulic fracture from the Bitterroot parent wells. The interpreted pore pressure from the BX2H DFIT provides a calibration point for the depleted area around the parent wells.

Fiber Optic Data

HFTS-2 demonstrated advanced FO technologies for stimulation and production monitoring with the first-of-a-kind three-fiber-wells design. Through near-wellbore surveys, Distributed Acoustic Sensing (DAS) and Distributed Temperature Sensing (DTS) data were acquired during stimulation of the two horizontal fiber wells (BX3H and BX4H). These data were used to quantify pumped fluid/proppant allocation among the clusters to estimate cluster efficiency for different completion designs. During the production phase, Distributed Strain Sensing (DSS) (Jin et al., 2021, Ugueto et al., 2021) data were acquired in the near-wellbore region, which allowed us to gain insights on time-dependent fracture property changes. Comprehensive analysis and evaluation of various completion designs using FO data are given by Zakhour et al. (2021) and Huckabee et al. (2022).

Through far-field surveys, cross-well strain rate data were obtained by the low-frequency DAS technique from all three fiber wells during stimulation of BX1H, BX2H, BX3H, BX4H and TR16H, which offered a great opportunity to gain better understanding of spatial (both horizontal and vertical) and temporal characteristics of hydraulic fracture propagation (for an example see Figure 5). Moreover, the interpreted frac hits and areal/vertical frac hits coverage on the three fiber wells provide valuable datapoints to calibrate subsurface models in high resolution. The FO-based MS monitoring was also conducted during child well stimulation and compared with the conventional MS data.

A fiber array was also installed in the vertical observation well, BX5P, which enabled observations of fracture height growth for the stages of the horizontal Boxwood wells that were on azimuth with BX5P (for an example see Figure 4). This data showed fracture growth extending upwards into the 2nd Bone Springs while downward propagation was general limited to the top of the Wolfcamp B. It is also clear from this data that there is extensive vertical fracture propagation occurring after the stage is shut-in. Each of these observations provide fracture geometry calibration points for the simulation model.

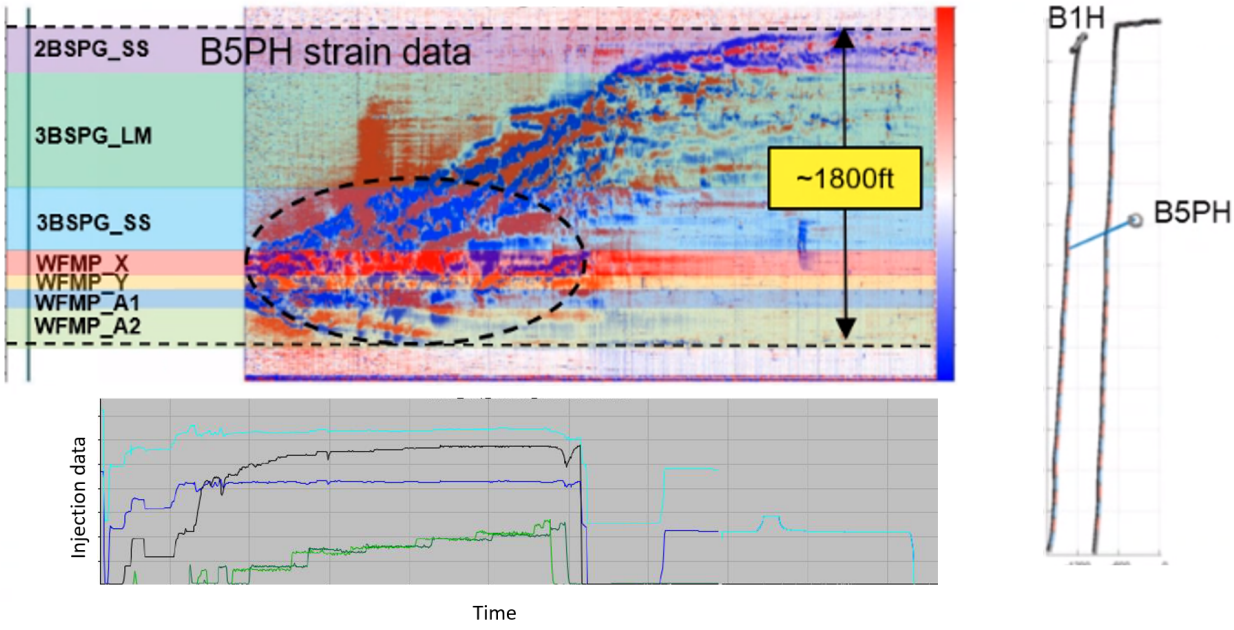

Figure 4 Example of fracture height growth as observed by the vertical observation well

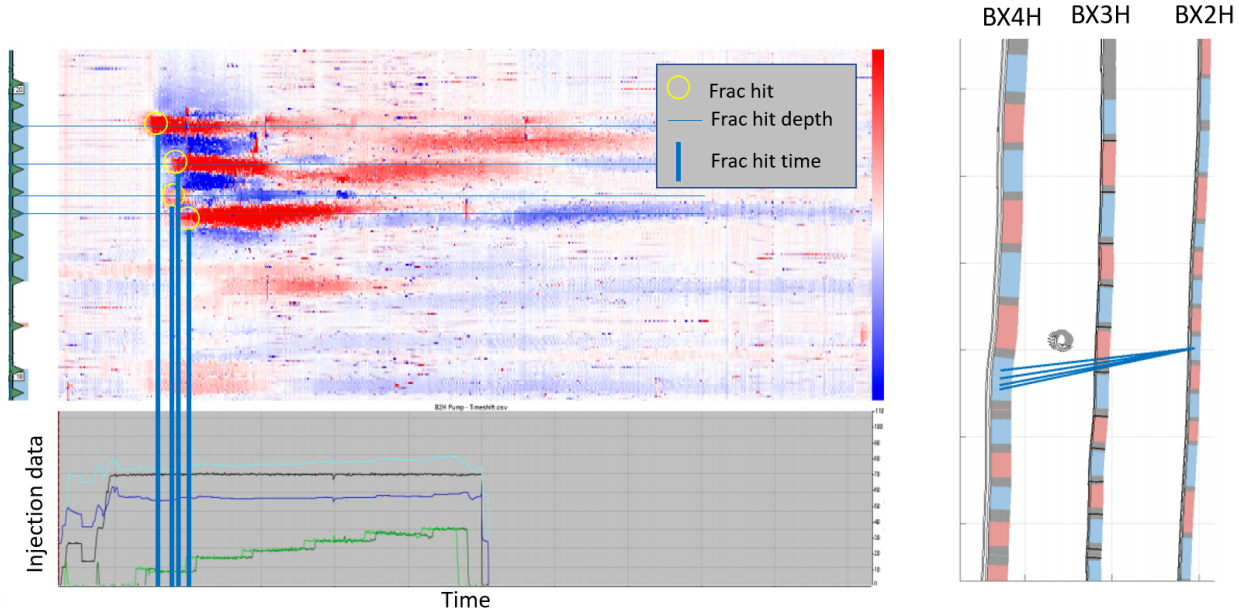

Figure 5 Example frac hit timing observed by the offset well fiber data

Bottomhole Gauges Data

The pressures from bottomhole gauges were another important part of the HFTS-2 dataset, quantifying the impact of frac hits and production depletion. 8 P/T gauges on the vertical well (B5PH) and 12 P/T gauges on the slant well (B6S) were installed spanning the formations from the 3rd Bone Spring Sand to the Wolfcamp-B. BX3H and BX4H have one heel P/T fiber gauge and one toe P/T fiber gauge respectively, and the other child wells also have a bottomhole P/T gauge.

The slant well was drilled after the stimulation of the child wells, so the 8 vertical well gauges along with the child well gauges were analyzed during the stimulation. The pressure data analysis of all the gauges shows clear frac hits on the vertical well during the treatment of the child wells and the pressure response severity increases towards the shallower benches, indicating the preferential upward fracture growth tendency. During the production phase, pressure depletion was observed from the lower 3rd Bone Spring Sand all the way to the Wolfcamp-A1 based on the pressure gauges data on BX5PH and BX6S. There was moderate pressure depletion in Wolfcamp-A2, but no depletion in Wolfcamp-B (Table 1). More details of the gauge response during stimulation and production period can be found in Pudugramam et al. (2021).

Well Interference Test Data

Two-well interference tests were conducted in the HFTS-2 area. In Feb. 2020, the first FO-based well interference and virtual production logging test was designed and executed based on a proprietary procedure developed by ConocoPhillips (Jin et al., 2019). This test was conducted to identify flow connections between BX4H and the offset well, and to estimate the production log from the FO data for BX4H. After a long, stable production period and an 18-hour shut-in period, all involved wells in this test were cycled shut-in or open for shorter intervals of a few hours. Through analysis of the DAS data acquired on BX4H, no identifiable well interference between BX4H and the offset wells was observed.

The second test in Sept. 2020 was a dedicated pressure interference test with longer shut-in and open time intervals (3-6 days) on the two child wells, BX3H and BX4H. The longer durations allowed enough time for pressure signals to reach the offset wells and offered a better chance to confirm the well communications after 7 months of production. Evident pressure response from shutting in and opening the BX3H and BX4H wells were picked up by 4 gauges in the vertical well B5PH and 8 gauges in the slant well B6S. The pressure signals at the gauges were weaker than the signals during the stimulation event.

Model Calibration Methods

The simulations for this study were performed with a combined hydraulic fracturing, wellbore, and reservoir simulator (McClure et al., 2022). Hydraulic fractures are represented discretely with planar elements; the well(s) are represented with linear elements; and the matrix is represented by volumetric elements using a rectilinear grid. The matrix mesh is non-conforming to the fracture elements; a submeshing technique is used to achieve numerical accuracy, even if the matrix mesh is coarse relative to the radius of investigation. In each timestep, the simulator enforces a set of balance equations: mass balance on fluid components, proppant types, and water solutes; energy balance; and (in the wellbore) momentum balance. In addition, the simulator solves the equations of linear elastic continuum mechanics to calculate the stress changes caused by fracture opening and by pressure and temperature changes in the matrix. All equations are solved simultaneously in every element in every timestep. Fracture propagation is based on linear elastic fracture mechanics, using the MuLTipEl algorithm developed by Dontsov et al. (2022). Stress interaction between fracture elements is calculated using the displacement discontinuity method from Shou et al. (1997).

Model Configuration

All modeling projects must balance model resolution and computational efficiency. We used a ‘sector’ model of a few stages along each well. This ensured the model accurately represented the scale of the data observed in the field and kept run times short enough to enable an iterative history matching process. This resulted in a model containing 2 to 3 representative stages from each well that were coincident with the vertical observation well to maximize the calibration potential of the data acquired in that well. The primary model focused on the North sector (see Figure 2) and included the four Boxwood wells, BX1H to BX4H. A 2nd sector model was used to validate the history match of the primary model. This model

included the two legacy Bitterroot wells and accounted for the interaction between wells of different generations.

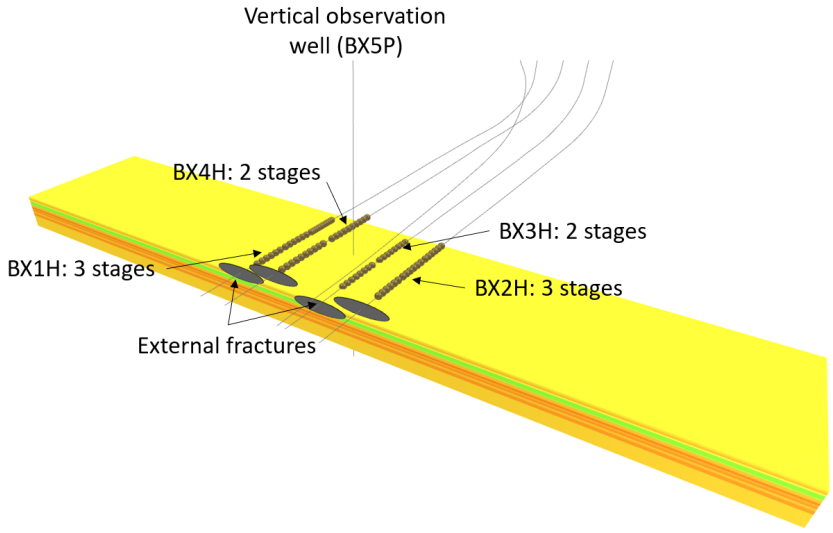

Figure 6 Model Configuration (brown spheres represent perforation clusters)

To account for stress shadow from prior stages that were not included in the model, 'external fractures' were added to each well on the toe side of the model. This ensured that the model accurately reflected initial stress state near the wellbore for each stage included in the model.

The variation of least principal stress, Shmin, with depth is a key input for any hydraulic fracture simulation model. In this work we applied the viscoelastic stress relaxion method to estimate the initial Shmin stress profile. The VSR technique uses a geomechanical model based on viscoelastic stress relaxation in relatively clay-rich rocks, to predicting continuous Shmin variations with depth. The method uses geophysical log data and Shmin measurements from routine diagnostic fracture injection tests (DFITs) at several depths for calibration (Singh, 2022). We computed a continuous stress profile as a function of the well logs that fit all the available DFITs.

The matrix grid was populated with petrophysical properties from the logs acquired in the vertical observation well. Landing depths for each well were corrected slightly to land the wells correctly in the model's rectilinear grid, which did not account for the slight dip of the formation. Injection sequences were generated to closely reflect the fluids and proppant that was pumped on a stage-by-stage basis. While on production, the wells were controlled by bottomhole pressure. BHP measurements were available in some cases, and in other cases, BHP was estimated from measured tubing head pressure.

History Matching Objectives

The totality of the diagnostic data was summarized into a list of 'key observations.' This list of observations was organized into a 'history matching plan,' in which we laid out which variables would be changed to match the observations and assessed the order in which the observations would be matched. The history match was relatively 'low dimensional,' in the sense that only a small number of global parameters were varied to achieve a match. By keeping the number of matching parameters relatively low, we reduce the potential for model overfit.

Model Calibration Results

The model was calibrated to the following areas of observations: fracture geometry (height and length), fracture propagation speed, cluster efficiency, ISIPs, pressure depletion by zone, production data (oil, gas, and water production), and well productivity vs time (RTA plots).

Fracture Geometry Calibration

It was necessary to reduce the pore pressure gradient in the Bone Springs because changing other geomechanical properties, such as vertical toughness, was not sufficient to encourage the degree of vertical fracture propagation observed by the microseismic and fiber in the vertical observation well. The original Shmin profile assumed that the pore pressure gradient in the Bone Springs was the same as the upper Wolfcamp. However, there is evidence that in this part of the Delaware Basin, there is a pressure ramp at the Wolfcamp-Bone Springs interface with the shallower zone being lower pressure (Rittenhouse et al. 2016, Popielski 2019, Dvory and Zoback 2021). Once the Bone Springs pore pressure was reduced, the model fracture heights were closer to the field observations. Introducing the Viscoelastic Stress Relaxation (VSR) Shmin profile into the model provided the final change necessary to match the upwards height growth of the fractures. This was because the calibrated VSR profile resulted in a higher Shmin estimate for the upper Wolfcamp (compared to the Easton Shmin estimate). This larger change in Shmin at the base of the Bone Springs (Figure 7, left panel) resulted in upwards fracture propagation all the way up to the 2nd Bone Springs (Figure 9), matching the observations from the vertical well fiber data (Figure 8).

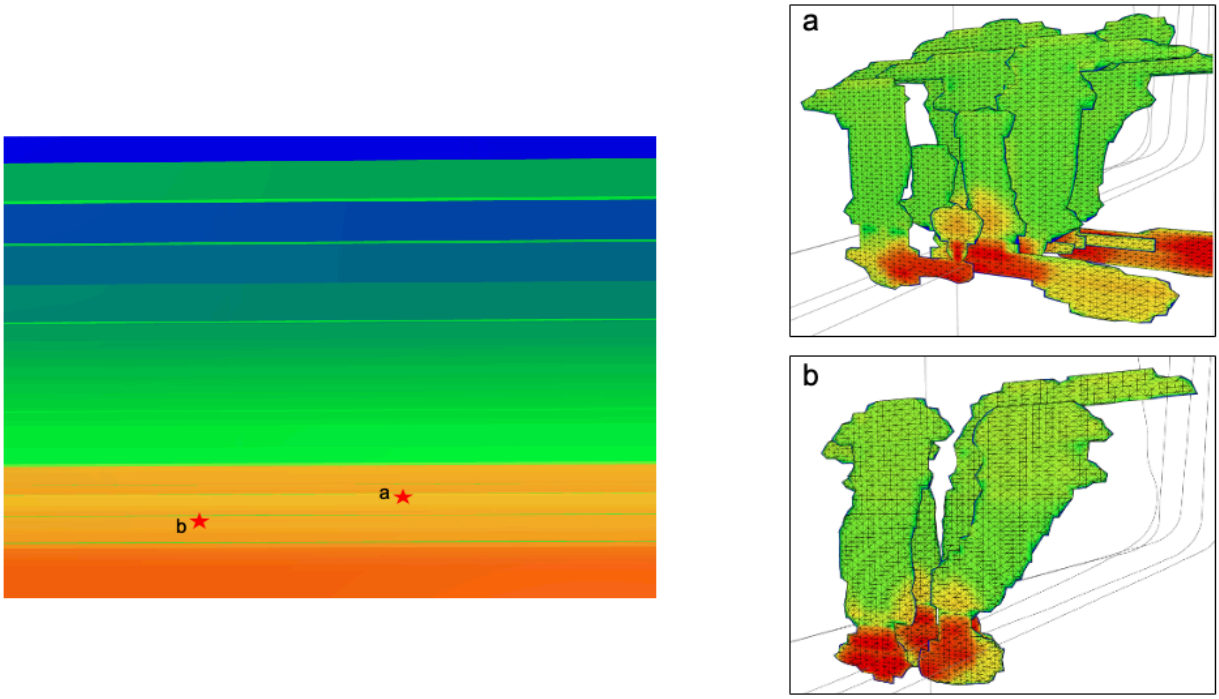

Figure 7 Different fracture geometry observed between two wells in the model alongside the initial Shmin in the model (left)

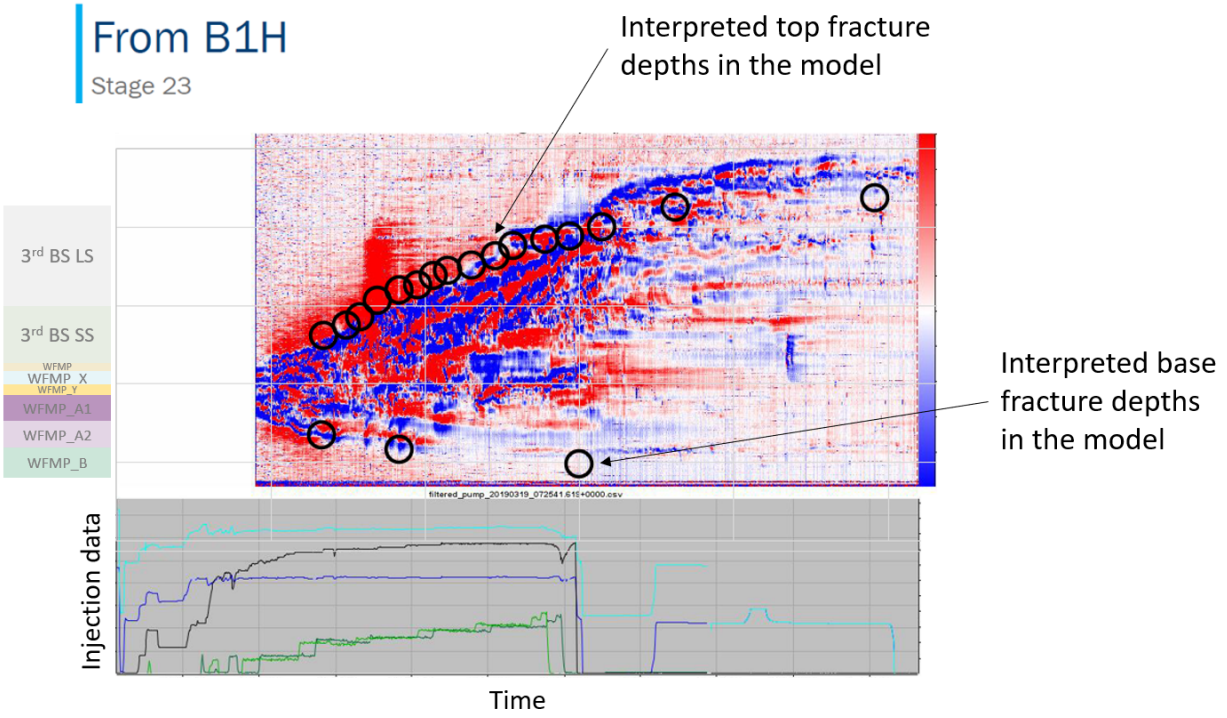

Figure 8 Model match to vertical fracture propagation observations

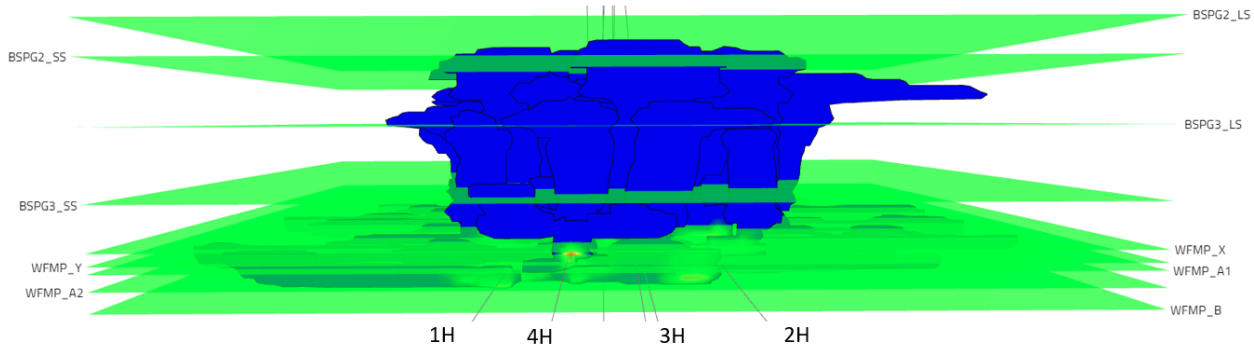

Figure 9 Total fracture heights in the model extending up into the 2nd Bone Springs Limestone

Fracture Propagation Speed

Horizontal fracture propagation rates were matched to the fracture arrival times in the offset fiber data by adjusting initial horizontal toughness by stratigraphic layer with toughness decreasing 70% from the top of Wolfcamp A1 to the top of the Wolfcamp Y. Additionally, toughness, viscous pressure drop and leak-off effects were accounted for using 3 strands per fracture per Fu et al (2020) and McClure et al (2022). This is equivalent to a 73% increase in toughness, a 9x increase in leakoff, and a 9x decrease in effective fracture conductivity during propagation. Figure 10 illustrates an example of first fracture arrival in the model compared to the observed data.

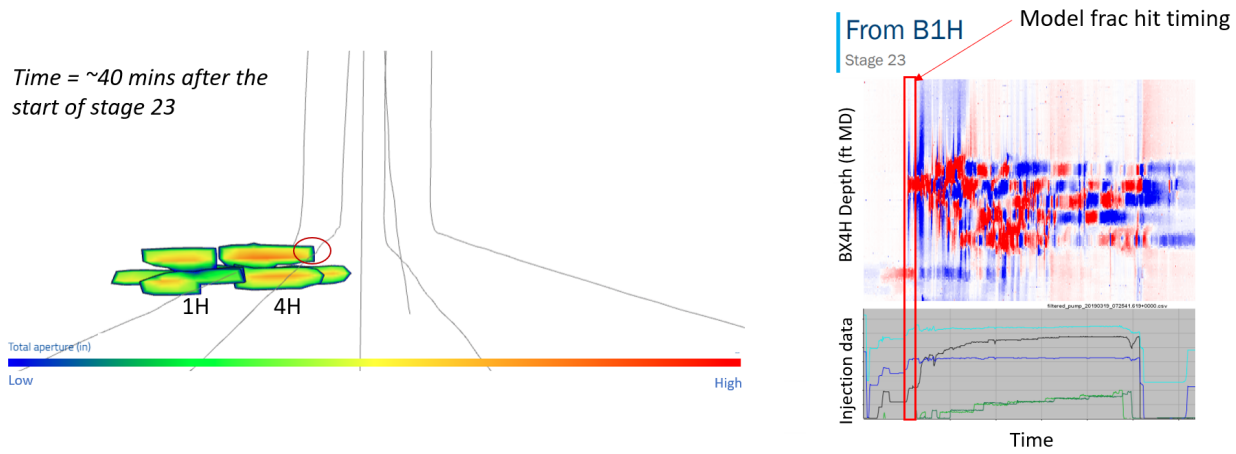

Figure 10 Frac hit timing match

Pressure Depletion Calibration

Permanent pressure gauges in the vertical observation well provided a measurement of relative depletion by layer over time (Figure 11). The pressure measurements in the vertical well are likely not directly connected to a conductive hydraulic fracture, rather these pressure measurements are offset by an unknown distance. This means the pressure measurements could yield a higher pressure measurement than the actual pressure in the conductive fractures at these depths. This effect can be seen in Figure 12 where the dashed line represents the range of possible pressure measurements a gauge could measure if the observation well were positioned differently relative to the hydraulic fracture network. By reading off the range of pressures along the dashed line in Figure 12, the model can be calibrated to the actual pressure data by ensuring that the actual data falls within the range observed (Table 1) along the dashed line in the model.

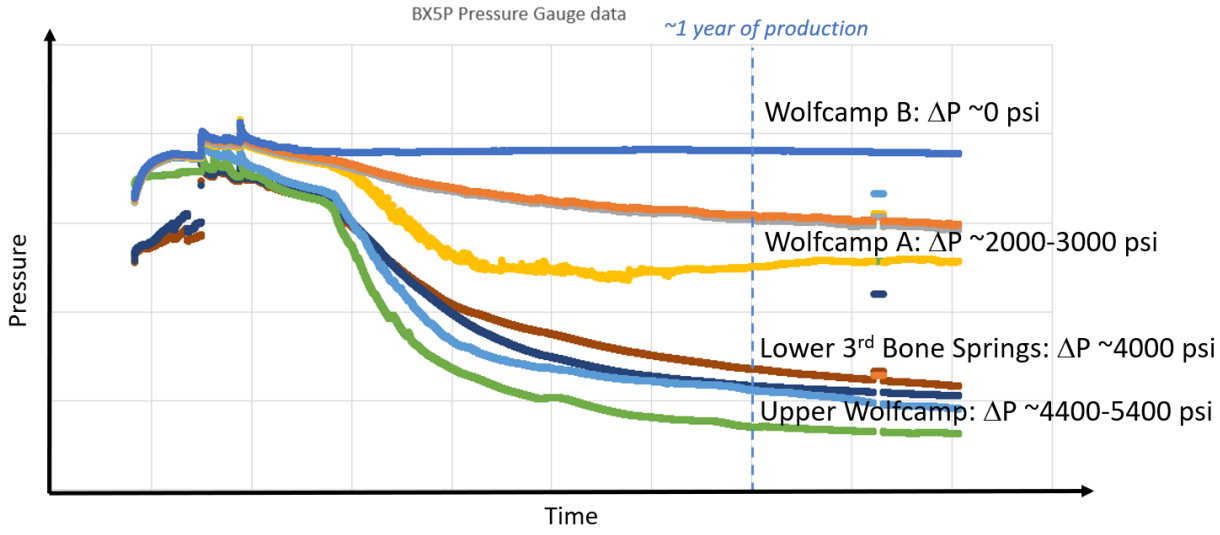

Figure 11 Pressure depletion observed by layer over time

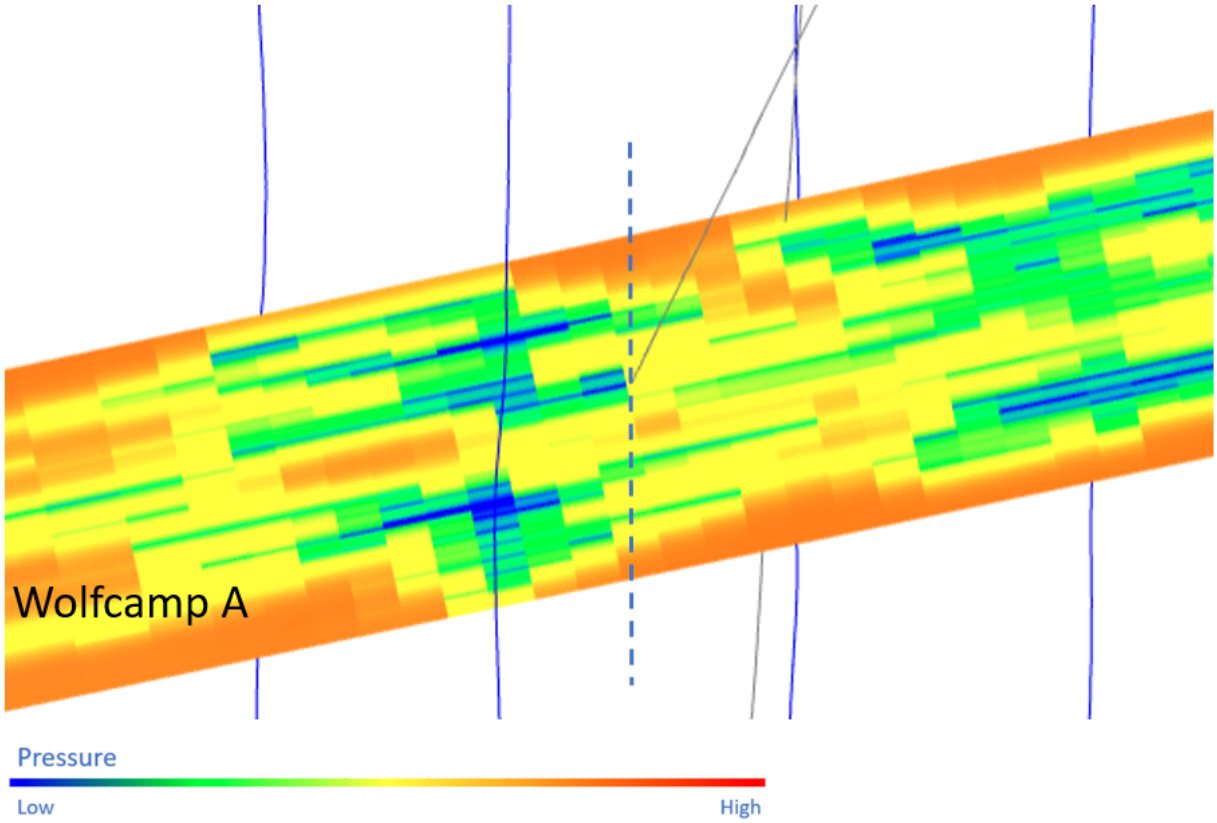

Figure 12 Example pressure depletion in the model – Wolfcamp A (after 1 year of production). The dashed line represents the range of possible pressure measurements a gauge could measure if the observation well were positioned differently relative to the hydraulic fracture network.

Zone	BX5P Gauge Measurements	Simulation Model Range	Match Status
3rd Bone Springs	~4,000 psi ΔP	~3,500 psi to 4,200 psi ΔP	Matched
Upper Wolfcamp	~5,000 psi to 6,000 psi ΔP	~3,000 psi to 6,000 psi ΔP	Matched
Wolfcamp A	~2,000 psi to 3,000 psi ΔP	~0 psi to 3,000 psi ΔP	Matched
Wolfcamp B	~0 psi ΔP	~0 psi ΔP	Matched

Table 1 Comparison of model depletion to pressure gauge observations

Productivity Calibration

Production data was history matched by varying a global permeability multiplier, relative permeability curves, pressure dependent permeability decline curves, and by increasing the permeability in the upper Wolfcamp to account for the observation that the wells landed in this zone had higher initial productivity. Figure 13 illustrates the overall production history match of the model compared to the actual data for total oil, gas, and water vs time. The RTA plot shown in Figure 14 illustrates the match to the change in

productivity for each well over time. A summary of the variables that were changed in the model to match the observed data is listed in Table 2.

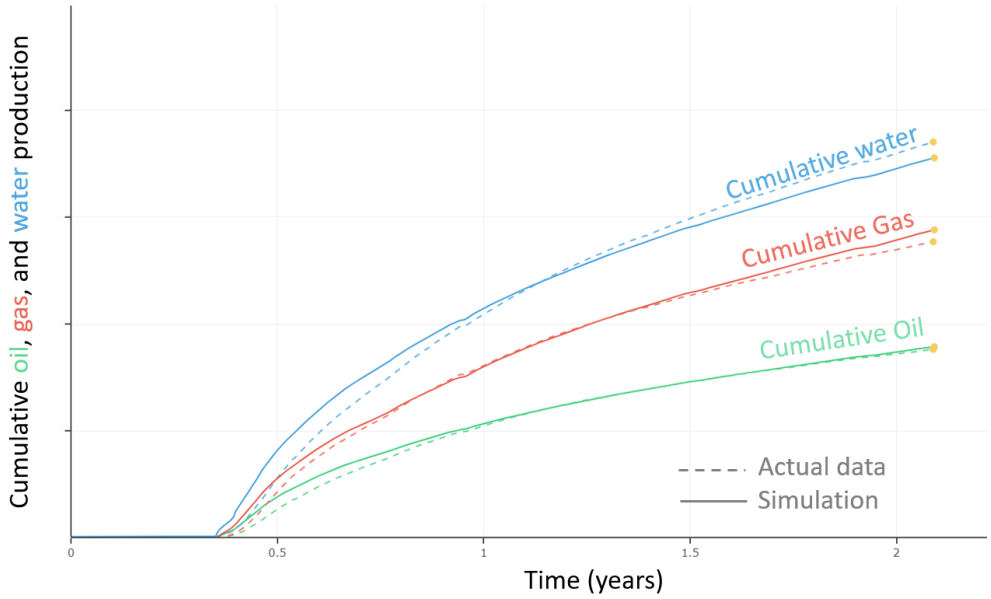

Figure 13 Production history match

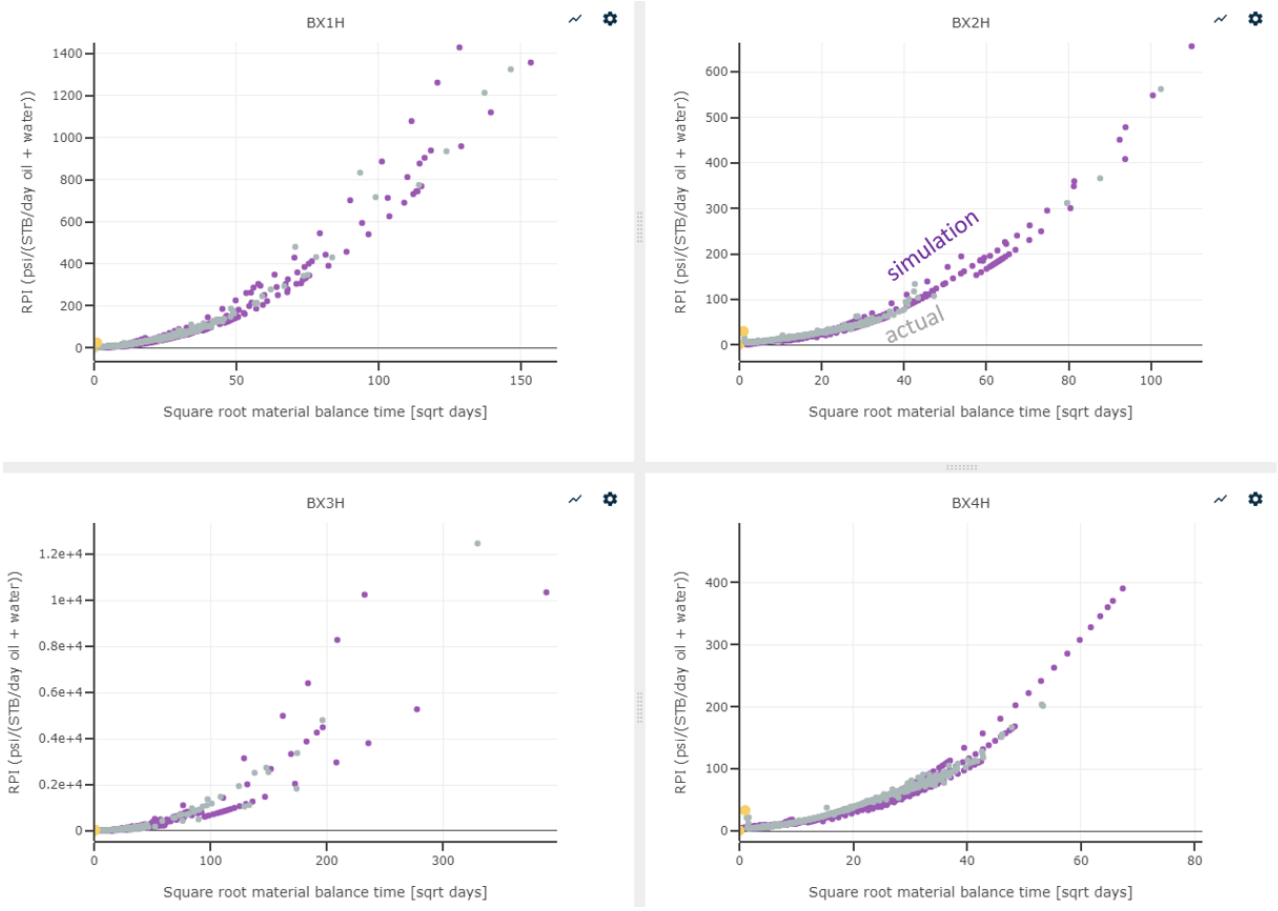

Figure 14 RTA history match for each well

Observation	Model Variable	Model Value
Fracture heights grow up into the 2nd Bone Springs (vertical well fiber)	Shmin profile, toughness	VSR* Shmin profile, Toughness profile.
Fracture propagation speeds to match fiber observations	Number of strands per fracture	3 strands; this is equivalent to a 73% increase in toughness, a 9x increase in leakoff, and a 9x decrease in effective fracture conductivity during propagation.
Initial Productivity	Global permeability multiplier	0.2
Relative productivity difference with landing depth	Wolfcamp X permeability multiplier	10
Productivity decline vs time	Pressure dependent permeability	2 exponential models (one for the upper and one for the lower Wolfcamp)
Water cut and GOR trends	Relative permeability curves.	

Table 2 Summary of model changes made to calibrate the model

Model Validation

A 2nd model was used to validate the history match of the primary model. The validation model was centered over the Southern sector (see Figure 2) and included the Bitterroot parent wells. The validation model matched the production data from both generations of wells.

The interpreted pressure from the BX2H DFIT provides an estimate of the parent well fracture pressure just before the child well fracturing operations. Visual inspection of the pressure in the model's parent well fractures shows a good agreement with the BX2H DFIT interpretation (Figure 15).

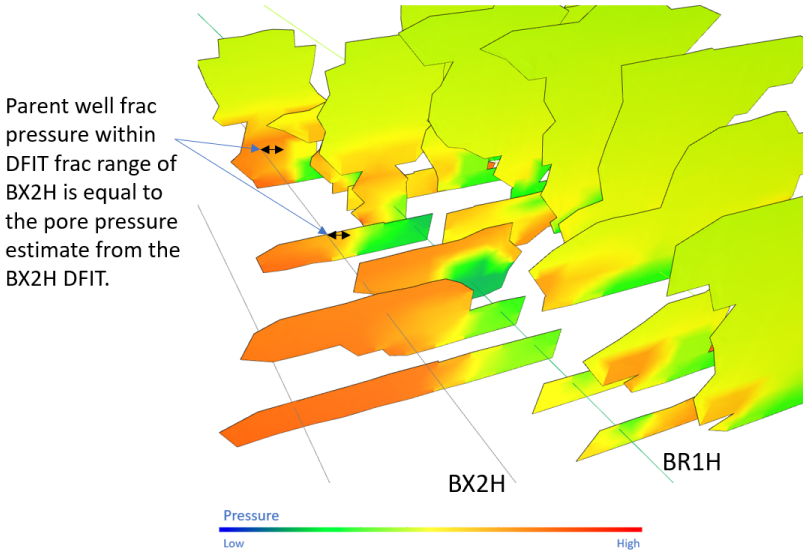

Figure 15 Validation model match to the pore pressure interpreted from the BX2H DFIT

Parent Well Influence on Fracture Asymmetry

Microseismic activity was observed to increase in the depleted region around the parent wells. This suggests that the child well fractures pressure up parent well fractures. In the validation model, the child well fractures intersect with the parent well fractures resulting in an increase in the pressure of the depleted parent well fractures, matching the observation from the microseismic.

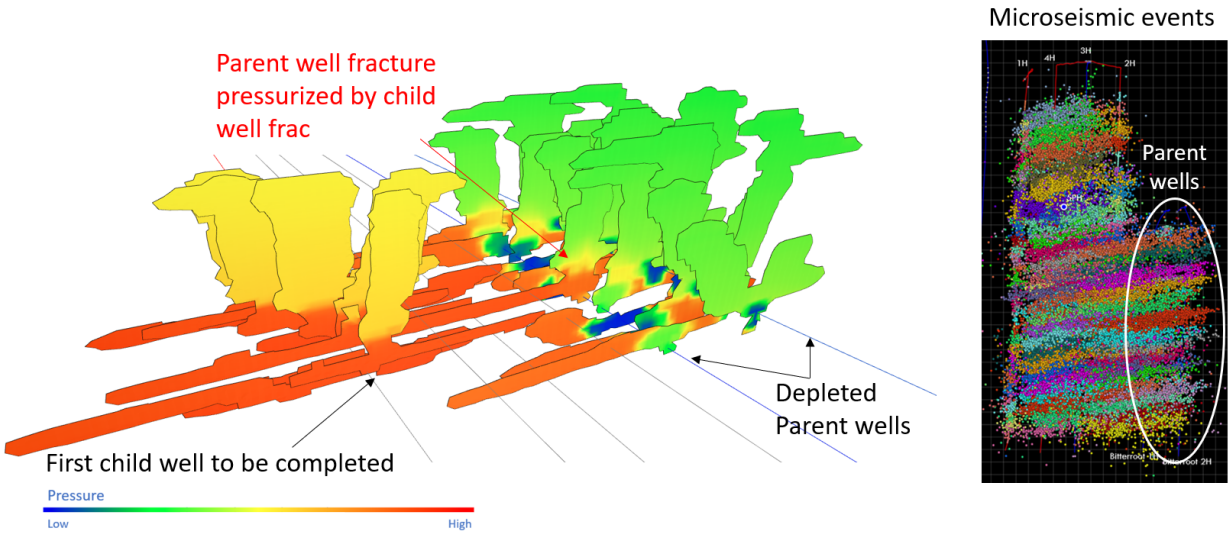

Figure 1 The right panel shows increased microseismic activity in the depleted region around the parent wells suggesting that the child well fractures are pressuring up the parent well fractures. The left panel shows the first stage of the first child well in the model pressuring up a depleted parent well fracture.

Optimization Methods

Optimization of well spacing, landing depth and completion design parameters was conducted using an automated optimization workflow. Objective function evaluations in the optimization problem are evaluated with forward runs of the fracturing/wellbore/reservoir simulator. The workflow employs a proxy model to improve computational speed and applies experimental design and Bayesian sampling techniques to generate points with which to train the proxy model (Kang et al., 2022).

The following variables were input as parameters in the modeling software's automated optimization workflow:

- Well spacing
- Cluster spacing
- Perforation friction
- Proppant Loading (lb/ft)
- Injection rate
- Fluid loading (bbl/ft)
- Landing depth

228 simulations were automatically generated over 3 generations with each generation increasing the resolution around the optimal outcomes. These simulations were then used to generate a proxy model with 1000 points to assess the impact of each variable on the objective function, Net Present Value (NPV)/section.

Optimization Results

The optimization results demonstrate that well spacing and landing zone are the primary drivers of performance due to their impact on effective drainage area. Proppant loading and cluster spacing are secondary performance drivers due to their contribution to fracture conductivity and effective fracture length.

The impact of landing depth on NPV/section is shown below in Figure 17 (left panel). The proxy model shows a clear optimal outcome when the wells are landed near the base of Zone 3. The impact of well spacing on NPV/section also shows an optimal outcome with a clear maximum as illustrated in Figure 17 (right panel).

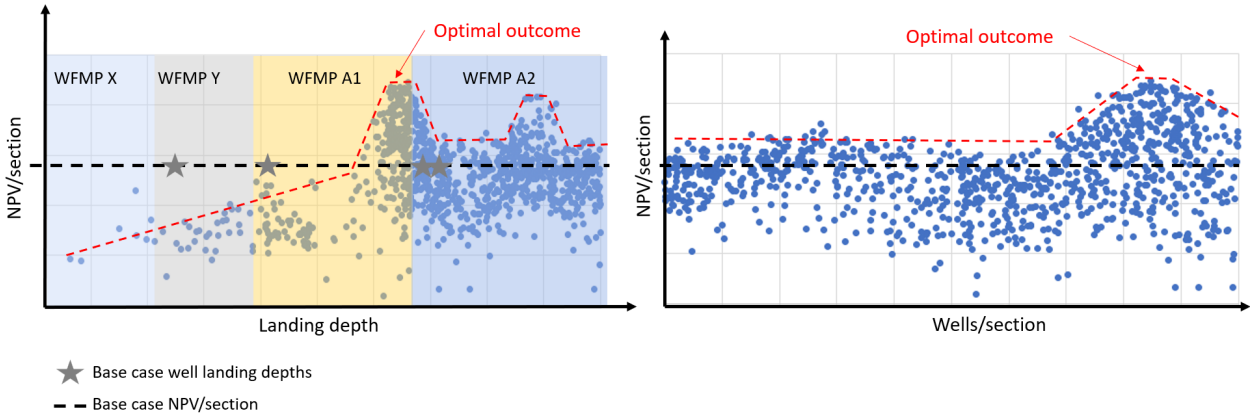

Figure 17 Proxy model results of NPV/section vs landing depth (left) and well spacing (right)

When well spacing is fixed at the optimal value (in the proxy model), the optimal cluster spacing and proppant loading, for that well spacing, can be predicted. This is illustrated in Figure 18.

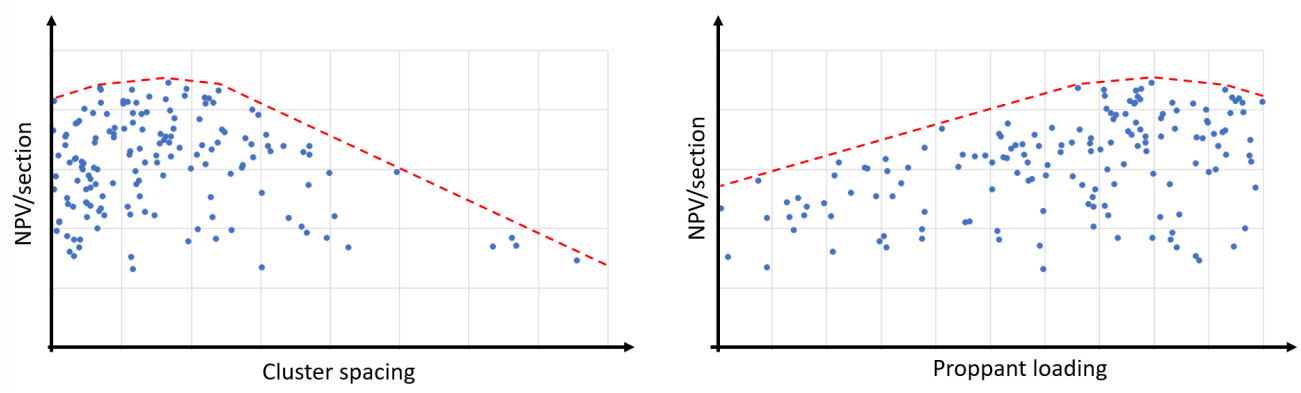

Figure 18 Proxy model results - NPV/section vs Cluster spacing and Proppant loading at the optimal Well spacing

Discussion of Optimization Results

It is instructive to compare the optimal design with the base case design to understand the reasons why the optimized design outperforms other designs. Well spacing and landing depth were observed to have the greatest impact on economic performance. As illustrated in Figure 20, this is primarily due to improved drainage of the main pay zone. The panels on the left show the pressure in the main pay zone after 30 years of production with warm colors representing higher pressure, un-depleted regions. The righthand

panel illustrates the fracture geometry with warmer colors containing more proppant and dark blue representing unpropped fracture area.

From the images of fracture geometry, we observe that landing the wells at the optimal landing depth results in less ineffective fracture growth up into the Bone Springs (which is not considered productive at this location due to its high water saturation and low pore pressure). This results in more effective vertical drainage of the pay zone and minimizes capital spent on injecting fluids that create unproductive height growth.

Due to the propensity for upwards fracture propagation, there is a limit to the effective drainage distance that can be achieved laterally. As a result, NPV can be increased with a tightened well spacing. The apparent limit in effective drainage distance is also evident in Figure 19 which shows that economic performance vs proppant loading has a clear maximum. In other words, NPV/section does not continue to increase beyond the optimal proppant loading value.

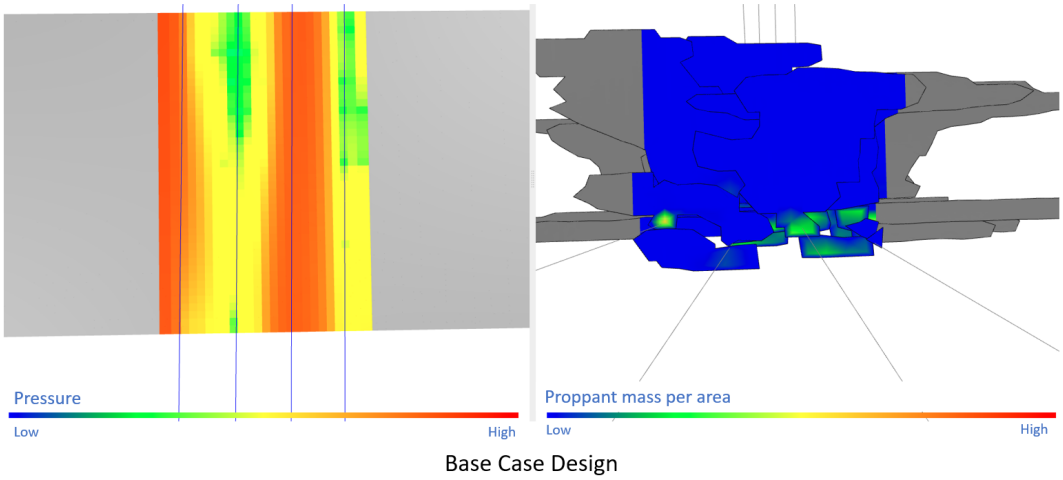

Figure 20 The left panel shows the distribution of pressure in the pay zone after 30 years of production in the Base Case model. The right panel shows the fracture geometries for the Base Case model.

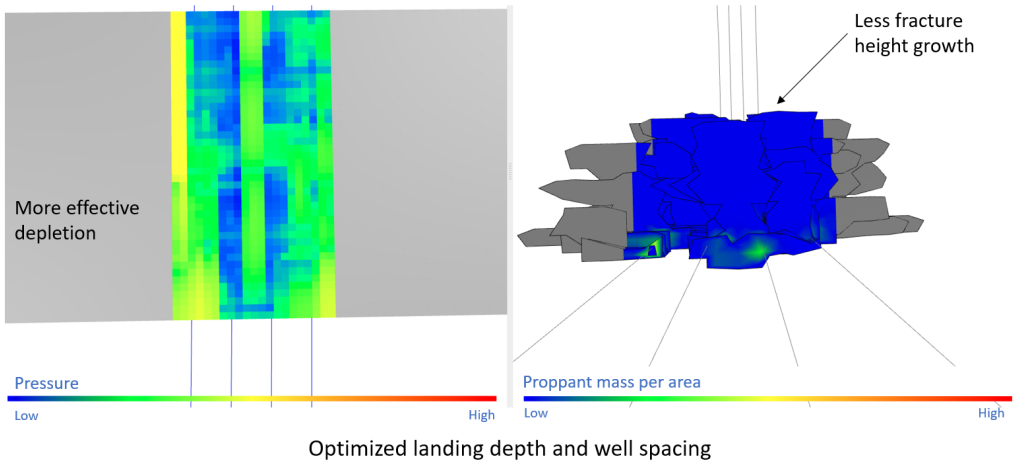

Figure 21 The left panel illustrates improved drainage from the main pay zone for the optimal NPV/section model. The right panel shows that the optimal NPV/section model has less height growth up into the unproductive Bone Springs.

Conclusions

This work demonstrates how high-quality field diagnostics can be synthesized with numerical models to help operators optimize well spacing and completion design. Leveraging the HFTS-2 dataset, a fully coupled hydraulic fracturing, reservoir, and geomechanics simulator was calibrated to the following categories of observations: fracture geometry (height and length), fracture propagation speed, cluster efficiency, ISIPs, pressure depletion by zone, production data (oil, gas, and water production), and well productivity vs time (RTA plots). This resulted in a well constrained model that was used to test hundreds of development schemes (well spacing, landing depth and completion design) to maximize the value of future analogous developments.

The optimization results demonstrate that well spacing and landing zone are the primary drivers of economic performance due to their impact on effective drainage area. Proppant loading and cluster spacing are secondary performance drivers due to their contribution to fracture conductivity and effective fracture length. The optimized design results in a 60% increase in NPV/section over the base case design.

These model driven hypotheses can now be field tested increasing the likelihood of success of field trials in future developments, steepening the learning curve and increasing the value operators can extract from their acreage positions in unconventional plays.

Acknowledgements

The authors would like to thank the following companies and organizations for their contributions the HFTS-2 project and for their support of this work: Occidental, GTI, the Department of Energy, Shell Exploration and Production Company, Stanford University, and the other member companies of the HFTS-2 consortium (BPx, Chevron, Concho, ConocoPhillips, Coterra, Devon, Diamondback, EcoPetrol, Jetta, Oasis, PDC, XTO). Special thanks to GTI for their stewardship of this multi-company research effort.

DOE Acknowledgment: "This material is based upon work supported by the Department of Energy under Award Number DE-FE0031577."

References

Bessa, F., Jerath, K., Ginn, C., Johnston, P., Zhao, Y., Brown, T., Lopez, R., Kessler, J., Nicklen, B., and Sahni, V. 2021. Subsurface Characterization of Hydraulic Fracturing Test Site-2 (HFTS-2), Delaware Basin. Presented at the Unconventional Resources Technology Conference, Houston, Texas, 26–28 July. URTEC-2021-5243-MS. https://doi.org/10.15530/urtec-2021-5243.

Ciezobka, Jordan. 2021. Overview of Hydraulic Fracturing Test Site 2 in the Permian Delaware Basin (HFTS-2). Presented at the Unconventional Resources Technology Conference, Houston, Texas, 26–28 July. URTEC-2021-5514-MS. https://doi.org/10.15530/urtec-2021-5514.

Dontsov, E., Hewson, C., and McClure, M. 2022. A new crack propagation algorithm that enables accurate simulation of propagation across thin layers in a practical field-scale fracturing model. Paper

SPE 209146-MS presented at the SPE Hydraulic Fracturing Technology Conference, The Woodlands, TX. https://doi.org/10.2118/209146-MS.

Dvory, N., and Zoback, M. 2021. Prior oil and gas production can limit the occurrence of injection-induced seismicity: A case study in the Delaware Basin of western Texas and southeastern New Mexico, USA. Geology 2021; 49 (10): 1198–1203. https://doi.org/10.1130/G49015.1.

Fu, W., Morris, J., Fu, P., Huang, J., Sherman, C., Settgast, R., Wu, H., Ryerson, F. 2020. Developing upscaling approach for swarming hydraulic fractures observed at Hydraulic Fracturing Test Site through Multiscale Simulations. Paper SPE-199689-MS presented at the SPE Hydraulic Fracturing Technology Conference and Exhibition, The Woodlands, TX. https://doi.org/10.2118/199689-MS.

Grechka, V., Howell, B., Li, Z., Furtado, D. and Straus, C. 2021. Microseismic at HFTS2: A Story of Three Stimulated Wells. Presented at the Unconventional Resources Technology Conference, Houston, Texas, 26–28 July. URTEC-2021-5517-MS. https://doi.org/10.15530/urtec-2021-5517.

Gale, J.F.W., Elliot, S.J., Rysak, B.G., Ginn, C.L., Zhang, N., Meyers, R.D., and Laubach, S.E. 2021. Fracture Description of the HFTS-2 Slant Core, Delaware Basin, West Texas. Presented at the Unconventional Resources Technology Conference, Houston, Texas, 26–28 July. URTEC-2021-5175-MS. https://doi.org/10.15530/urtec-2021-5175.

Huckabee, P., Ugueto, G., Haustveit, K., Wojtaszek, M., Mondal, S., Ledet, C., Daredia, T. and Reynolds, A. 2022. Completions and Stimulation Experimental Design, Execution, Analysis & Application for the Permian Delaware Basin Hydraulic Fracture Test Site 2. Presented at the Hydraulic Fracturing Technology Conference and Exhibition, The Woodlands, Texas, 2–4 February. SPE-209172-MS. https://doi.org/10.2118/209172-MS.

Jin, G., Ugueto, G., Wojtaszek, M., Guzik, A., Jurick, D., and Kishida, K. 2021. Novel Near-Wellbore Fracture Diagnosis for Unconventional Wells Using High-Resolution Distributed Strain Sensing during Production. *SPE J.* **26** (05): 3255–3264. SPE-205394-PA. https://doi.org/10.2118/205394-PA.

Jin, G., Friehauf, K., Roy, B., Constantine, J.J., Swan, H.W., Krueger, K.R., and Raterman, K.T. 2019. Fiber Optic Sensing-Based Production Logging Methods for Low-Rate Oil Producers. Presented at the Unconventional Resources Technology Conference, Denver, Colorado, 22–24 July. URTEC-2019-943-MS. https://doi.org/10.15530/urtec-2019-943.

Kang, C., McClure, M., Reddy, S., Naidenova, M., and Tyankov, Z. 2022. Optimizing Shale Economics with an Integrated Hydraulic Fracturing and Reservoir Simulator and a Bayesian Automated History Matching and Optimization Algorithm. Presented at the SPE Hydraulic Fracturing Technology Conference and Exhibition, The Woodlands, Texas, USA, February 2022. SPE-209169-MS https://doi.org/10.2118/209169-MS

Maity, D. and Ciezobka, J. 2021. A Systematic Interpretation of Subsurface Proppant Concentration from Drilling Mud Returns: Case Study from Hydraulic Fracturing Test Site (HFTS-2) in Delaware Basin. Presented at the Unconventional Resources Technology Conference, Houston, Texas, 26–28 July. URTEC-2021-5189-MS. https://doi.org/10.15530/urtec-2021-5189.

McClure, M., C. Kang, S. Medam, C. Hewson, and E. Dontsov. 2022 ResFrac Technical Writeup. [Online]. Available: https://arxiv.org/abs/1804.02092.

Popielski, A. 2019. Pore Pressure Estimation in Complex Lithologies: A Novel Approach in Delaware Basin Wolfcamp. Paper presented at the SPE/AAPG/SEG Unconventional Resources Technology Conference, Denver, Colorado, USA, July 2019. https://doi.org/10.15530/urtec-2019-165.

Pudugramam, S., Zhao, Y., Bessa, F., Li, J., Zakhour, N., Brown, T., Han, J., Harmawan, I., and Sahni V. 2021. Analysis and Integration of the Hydraulic Fracturing Test Site-2 (HFTS-2) Comprehensive Dataset.

Presented at the Unconventional Resources Technology Conference, Houston, Texas, 26–28 July. URTEC-2021-5241-MS. https://doi.org/10.15530/urtec-2021-5241.

Rittenhouse, S., Currie, J., and Raleigh B. 2016. Using Mud Weights, DST, and DFIT Data to Generate a Regional Pore Pressure Model for the Delaware Basin, New Mexico and Texas. Paper presented at the SPE/AAPG/SEG Unconventional Resources Technology Conference, San Antonio, Texas, USA, August 2016. https://doi.org/10.15530/URTEC-2016-2450423.

Shou, K., Siebrits, E., Crouch, S. 1997. A higher order displacement discontinuity method for three-dimensional elastostatic problems. International Journal of Rock Mechanics and Mining Sciences 34 (2): 317-322, https://doi.org/10.1016/S0148-9062(96)00052-6.

Singh, A., and Zoback, M. 2022. Predicting variations of the least principal stress with depth: Application to unconventional oil and gas reservoirs using a log-based viscoelastic stress relaxation model. Geophysics, Vol. 87, No. 3 (May-June 2022); p. 1–12. https://doi.org/10.1190/geo2021-0429.1.

Ugueto, G.A., Wojtaszek, M., Mondal, S., Guzik, A., Jurick, D. and Jin, G. 2021. New Fracture Diagnostic Tool for Unconventionals: High-Resolution Distributed Strain Sensing via Rayleigh Frequency Shift during Production in Hydraulic Fracture Test 2. Presented at the Unconventional Resources Technology Conference, Houston, Texas, 26–28 July. URTEC-2021-5408-MS. https://doi.org/10.15530/urtec-2021-5408.

Zakhour, N., Jones, M., Zhao, Y., Orsini, K., and Sahni, V. 2021. HFTS-2 Completions Design and State-of-the-Art Diagnostics Results. Presented at the Unconventional Resources Technology Conference, Houston, Texas, 26–28 July. URTEC-2021-5242-MS. https://doi.org/10.15530/urtec-2021-5242.

Zhao, Y., Bessa, F., Sahni, V., Pudugramam, S. and Liu, S. 2021. Key Learnings from Hydraulic Fracturing Test Site-2 (HFTS-2), Delaware Basin. Presented at the Unconventional Resources Technology Conference, Houston, Texas, 26–28 July. URTEC-2021-5229-MS. https://doi.org/10.15530/urtec-2021-5229.